Progress In Electromagnetics Research M, Vol. 116, 65–75, 2023

Three-Dimensional Near-Field Pattern Shaping Antenna Array with Arbitrary Focus Configuration

Qiaojiang Xia, Xiao Cai*, Zhu Duan, and Wen Geyi

Abstract—In this paper, a 24-element microstrip antenna array with three-dimensional near-field pattern shaping capability for microwave hyperthermia is presented. The antenna array operating at 2.45 GHz is designed based on the weighted constrained method of the maximum power transmission efficiency (WCMMPTE). By setting proper constraints for the electric field distribution of several selected points within the target area, the three-dimensional (3D) shape of the electric field can be characterized, meanwhile ensuring that the power is maximally concentrated in this area. Moreover, the shape, size, and spatial location of the three-dimensional area are all adjustable according to the selection of those specific points, making the array quickly adaptable for different actual requirements. The electric field distribution of the preset 3D shape can be focused at center or off-center with optimized excitations fed into the array. The measured electric field distribution shows that the transmitting array antenna is able to achieve a preset 3D shape of the electric field distribution as well as a preset offset position in the desired direction, agreeing very well with the simulations.

1. INTRODUCTION

Near-field focusing has been developing rapidly and attracted wide attention in various applications recently, e.g., wireless power transfer [1, 2], RFID [3], and biomedical applications including lithotripsy [4] and microwave hyperthermia [5–9]. In these scenarios, the targets are in the near-field region of the antennas, therefore also requiring the electromagnetic power to be concentrated in the near-field region for higher system efficiency and accuracy.

In the past decades, while many strategies aimed at forming a single focus have been presented, such as time reversal [10], optimal constrained power focusing [11], and global optimization methods [12], few strategies have been put forward to generate a required 3D shape of the electric field distribution. In fact, in many cases a shaped field, rather than a focused one, is of interest. For example, in the treatment of microwave hyperthermia, the treatment of advanced tumors requires precise control of the spatial electric field intensity to deal with arbitrarily extended target areas.

In the near-field region, the 3 dB focal spot usually exhibits an elongated shape [13], where the depth of the focal spot is always larger than the width. In order to regulate the focal spot, Blanco et al. used the normal field component of an annular-slot leaky-wave antenna to supplement the tangential component around the focus area and obtained a more symmetric focus [14]. In [15], the shape of focus is controlled by the geometric and electrical parameters of the antenna array composed of multiple panels. The above scheme realizes the control of the fixed focus at center, but less publications are found in terms of the focus at off-center. In order to produce an electric field with a given spatial distribution of intensity, the time-reversal mirror in the target region has realized the configuration of the field in two-dimensional plane through the time-reversal method [16]. In [17], field formation in three-dimensional space is realized through the global optimization scheme of multiple target points.

Received 12 January 2023, Accepted 27 March 2023, Scheduled 4 April 2023
* Corresponding author: Xiao Cai (caixiao@nuist.edu.cn).
The authors are with the Nanjing University of Information Science and Technology, Nanjing 210044, China.

However, the whole system is expensive, and the corresponding optimization process is time-consuming. Furthermore, although the focusing field is formed, the system efficiency has not been optimized to the highest. The method of maximum power transmission efficiency (MMPTE) has been proposed to solve this problem and widely used in wireless power transfer systems, focused antennas, multi-beam antennas, beam formation, and other fields [18]. In [19], the weighted constrained method of the maximum power transmission efficiency (WCMMPTE) is used to realize the flat top formation of the far-field and near-field of array antennas. For the receiving antennas are indispensable for MMPTE and WCMMPTE to obtain the required scattering parameters, it is not convenient to place the receiving antennas in practical applications, such as in human body for biomedical treatment.

In this paper, the WCMMPTE is used for three-dimensional near-field shaping without using a receiving antenna in the target area, effectively reducing the pain of patients in the treatment of microwave hyperthermia. The ratio of the energy of the target area to the total input energy is taken as the optimization objective. In this way, the power can be maximally concentrated in the target area by selecting the proper spatial sampling points. For proof of concept, a 24-element antenna array with a multi-panel structure is designed and fabricated to realize a spherical distribution of 3 dB electric field in the target area at center or off-center.

2. DESIGN METHOD

According to the MMPTE reported in [18], if the transmitting antenna array needs to transmit electromagnetic energy to multiple areas designated by Ω_p $(p = 1, 2, \ldots, n)$, the ratio of the weighted sum of the radiated energies in these regions Ω_p over the total input power fed into the transmitting array may be introduced as the performance index, also termed as the power transmission efficiency (PTE):

$$\mathrm{PTE} = \frac{\sum_{p=1}^{n} \int_{\Omega_p} W_p(\mathbf{r}) |\mathbf{E}(\mathbf{r})|^2 d\Omega(\mathbf{r})}{P_{in}} \tag{1}$$

If the transmitting antenna elements are all matched, we have $P_{in} = ([a_t], [a_t])/2$, where $[a_t] = [a_1, a_2, \ldots, a_n]^T$ is the vector of the normalized incident waves for the transmitting array. The fields radiated from the transmitting antenna array can then be written as [18]:

$$\mathbf{E}(\mathbf{r}) = \sum_{j=1}^{m} a_j \mathbf{E}_j(\mathbf{r}), \mathbf{H}(\mathbf{r}) = \sum_{j=1}^{m} a_j \mathbf{H}_j(\mathbf{r}) \tag{2}$$

where $\mathbf{E}_j(\mathbf{r})$ and $\mathbf{H}_j(\mathbf{r})$ are the fields generated by the jth antenna element of the transmitting array, with the remaining ports terminated in matched loads. In order to maximize the transmission efficiency while constraining the energy allocation of multiple regions, we need to solve the following problem:

$$\begin{aligned} &\max \frac{[a_t]^H [A] [a_t]}{[a_t]^H [a_t]} \\ &s.t. \int_{\Omega_p} W_p(\mathbf{r}) \mathbf{E}_j(\mathbf{r}) \cdot \overline{\mathbf{E}_i(\mathbf{r})} d\Omega(\mathbf{r}) = [W][c] \end{aligned} \tag{3}$$

with $[A] = 2 \sum_{p=1}^{n} \int_{\Omega_p} W_p(\mathbf{r}) \mathbf{E}_j(\mathbf{r}) \cdot \overline{\mathbf{E}_i(\mathbf{r})} d\Omega(\mathbf{r})$, where $[W] = \mathrm{diag}(w_1, w_2, \ldots, w_p)$ is a weighting matrix introduced to adjust the power received by target area. The constraint in (3) controls the field pattern in the sampling point region, while the maximum PTE is guaranteed. The optimal solution of the above constrained problem (3) can be obtained as follows [19]:

$$[a_t] = [A]^{-1} [E]^H ([E][A]^{-1} [E]^H)^{-1} [W][c] \tag{4}$$

3. ANTENNA ARRAY DESIGN

The antenna array element is selected to be a square microstrip patch operating at 2.45 GHz, fabricated on a 1.6-mm-thick FR4 substrate ($\varepsilon_r = 4.4$, $\tan\delta = 0.02$). Its geometrical parameters are optimized by Ansys HFSS (High Frequency Structure Simulator), which is found to be $W_p = 28.2$ mm and $L_f = 8.98$ mm. The sketch of the patch element and its simulated and measured reflection coefficients ($|S_{11}|$) are shown in Figs. 1(a) and (b), respectively. Then three 4×2 subarrays ($W = 150.6$ mm and $L = 273$ mm) are built with an inter-element spacing of half wavelength. The multi-panel array structure is shown in Fig. 2.

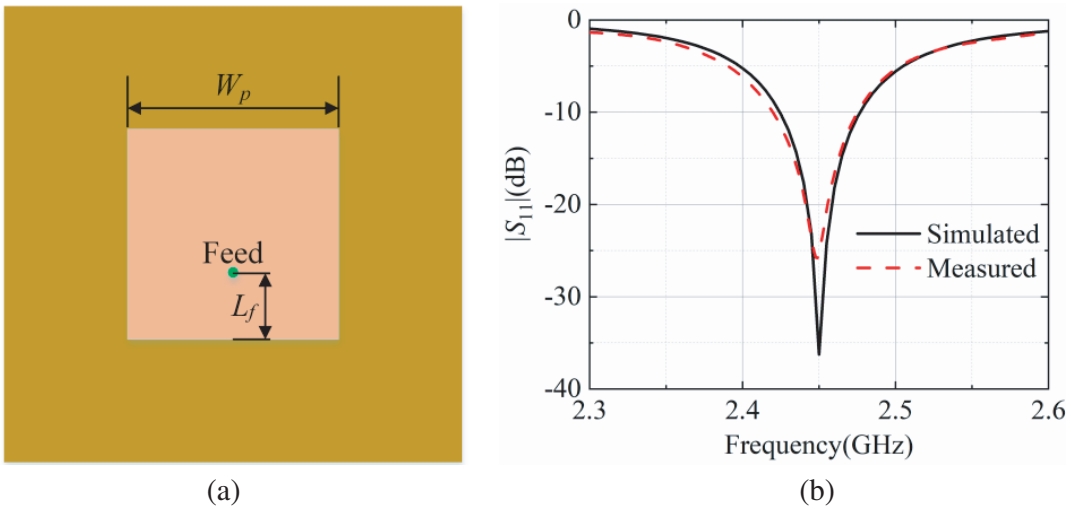

Figure 1. (a) Sketch of patch element and (b) the simulated and measured reflection coefficients of the patch element.

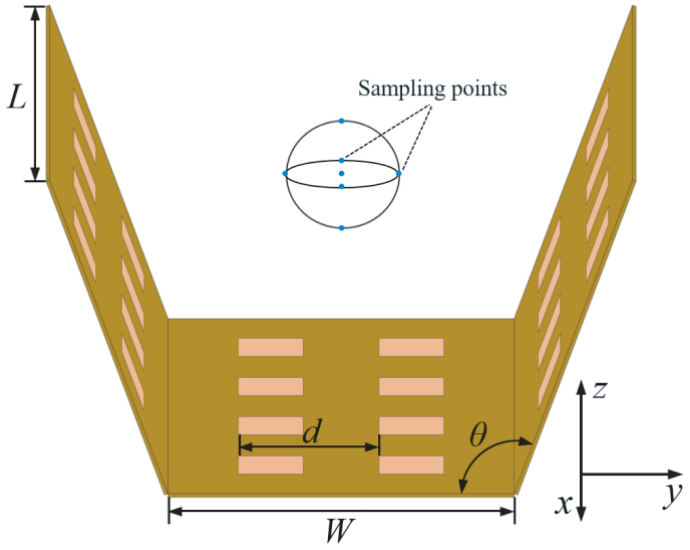

Figure 2. Sketch of the proposed near-field shaping antenna array with multi-panel structure.

As shown in Fig. 3 and Fig. 4, the intersection angle between subarrays will affect the 3D shape of the electric field distribution, especially along the vertical direction. When θ is 180°, the sizes of the focal spot on both xz-plane and yz-plane are relatively large, which can be seen in Figs. 3(a) and (b).

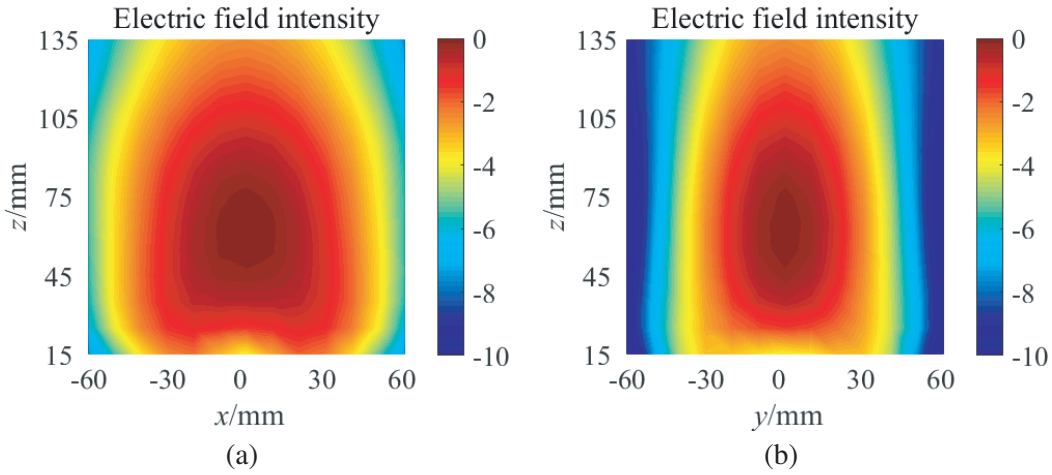

Figure 3. The normalized electric field distributions of the planar array for $\theta = 180°$. (a) xz-plane. (b) yz-plane.

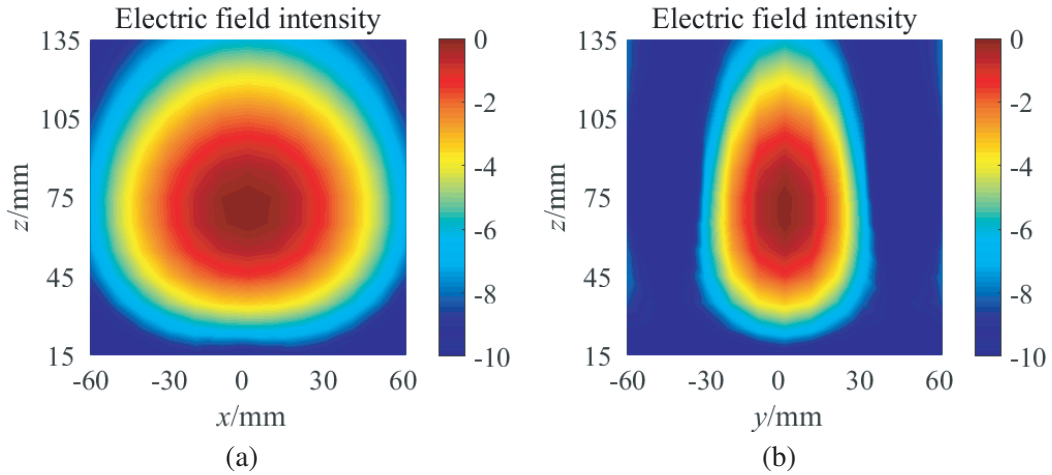

Figure 4. The normalized electric field distributions of the proposed array for $\theta = 110°$. (a) xz-plane. (b) yz-plane.

As shown in Fig. 4, when θ is changed to 110°, the size of the focal spot becomes smaller, which means that the radiated power is much more concentrated at the focal spot.

The transmitting array antenna is required to achieve not only a preset sphere-shaped electric field distribution, but also a preset offset position in the desired direction. Besides the focusing performance, the choice of the angle θ may also affect the deviation between the actually realized and the desired center positions of the sphere-shaped electric field.

As shown in Table 1, the deviations between the expected and actually realized center positions of the spherical electric field are compared with respect to the angle θ. When the center of the spherical electric field is expected to be at (10 mm, 0 mm, 75 mm) and (0 mm, 10 mm, 75 mm), the electric field is required to achieve an offset of 10 mm in the x-axis and y-axis directions, respectively. When θ is larger than 110°, the actual center position of the sphere-shaped electric field has a remarkable deviation from the expected one, especially when it is shifted along the y-axis. As θ increases from 120° to 180°, the deviation becomes larger until a spherical electric field cannot be formed in the target region. Hence, the final angle of θ is determined to be 110° in order to achieve both accurate center position of the spherical electric field and electric field shaping effect.

Table 1. The relationship between the angle θ and deviation between the expected and actually realized center position of the sphere-shaped electric field.

θ	Expected position along the x-axis	Actual position along the x-axis	Expected position along the y-axis	Actual position along the y-axis
90°	10 mm	9.6 mm	10 mm	6 mm
100°	10 mm	9.6 mm	10 mm	9.2 mm
110°	10 mm	10.3 mm	10 mm	9.56 mm
120°	10 mm	9.16 mm	10 mm	7.51 mm
180°	10 mm	Unable to shape	10 mm	Unable to shape

The three-dimensional near-field shaping procedure can be explained as follows. When the array model is determined, the electric field distribution of the sampling points in the target area can be obtained by HFSS. As shown in Fig. 2, in order to make the electric field generated by the transmitting array distribute as a sphere, the center of the sphere and other six points on the desired sphere are taken as the sampling points. We expect the transmitting array antenna to generate a spherical electric field at a height of 75 mm from the center of the array and to achieve an offset of 10 mm in the desired direction. Taking PTE as the optimization goal and introducing the electric field distribution of sampling points as the constraint conditions, the electric field concentrated in the spherical area is produced, and at the same time the PTE of the system is maximized. The optimized distribution of excitations (ODEs) can be calculated through Equation (4), as shown in Table 2, where P1 (0 mm, 0 mm, 75 mm) corresponds to the expected focus position coordinates of the electric field at the center, while P2 (0 mm, 10 mm, 75 mm) and P3 (10 mm, 0 mm, 75 mm) correspond to two different off-center cases.

The fabricated antenna array with 24 microstrip patch elements is shown in Fig. 5. In the experiment, the optimal excitations for 24 ports are realized by the feed circuit board, composed of one three-way microstrip power divider and three eight-way RF circuits consisting of several attenuators and phase shifters, as shown in Fig. 6. The total input power to the feeding circuit board is provided by port 1 of the vector network analyzer. The test probe of the high-precision near-field measurement system is connected to port 2. As a result, the electric field distribution in the target area can be measured and shown in the form of the scattering parameter S_{21} between the two ports. Since the synthesized electric field is only linearly polarized, the linearly-polarized test probe is always set to be horizontal during the whole test process. By moving the stepper, the electric field on different planes can be measured.

Figure 5. Fabricated antenna array.

Table 2. ODEs.

Antenna No.	P1	P2	P3
1	$0.14\angle -66.5$	$0.13\angle -58$	$0.12\angle -52.4$
2	$0.14\angle -66.1$	$0.15\angle -72.5$	$0.12\angle -51.7$
3	$0.31\angle -168$	$0.27\angle -161.4$	$0.26\angle -160$
4	$0.31\angle -168$	$0.34\angle -172.3$	$0.26\angle -160$
5	$0.32\angle -165.4$	$0.28\angle -158.5$	$0.36\angle -171.5$
6	$0.32\angle -165.5$	$0.36\angle -170.4$	$0.36\angle -171.6$
7	$0.14\angle -64$	$0.14\angle -56$	$0.17\angle -82.1$
8	$0.14\angle -64$	$0.15\angle -70.4$	$0.17\angle -82.6$
9	$0.13\angle -37.3$	$0.12\angle -52.2$	$0.17\angle -9.2$
10	$0.25\angle -61.9$	$0.21\angle 47$	$0.22\angle 78$
11	$0.15\angle 97.6$	$0.16\angle 75$	$0.15\angle 108.1$
12	$0.16\angle -81.1$	$0.2\angle -105.3$	$0.15\angle -57.3$
13	$0.17\angle 113.3$	$0.18\angle 102$	$0.16\angle 105.7$
14	$0.18\angle -63.7$	$0.17\angle -87.4$	$0.18\angle -84.4$
15	$0.12\angle -8.8$	$0.1\angle -28.7$	$0.07\angle -37.6$
16	$0.23\angle 52$	$0.21\angle 34.1$	$0.28\angle 37.6$
17	$0.25\angle 62$	$0.29\angle 72.2$	$0.23\angle 78.1$
18	$0.13\angle -37.1$	$0.16\angle -19.8$	$0.17\angle -10$
19	$0.16\angle -80.7$	$0.12\angle -55.3$	$0.15\angle -57.4$
20	$0.15\angle 98.6$	$0.12\angle 130.2$	$0.15\angle 109.4$
21	$0.18\angle -63.8$	$0.14\angle -37$	$0.18\angle -84.2$
22	$0.17\angle 113.3$	$0.15\angle 150.3$	$0.16\angle 107$
23	$0.23\angle 52$	$0.26\angle 71.6$	$0.27\angle 37.7$
24	$0.12\angle -9.1$	$0.17\angle 3.3$	$0.06\angle -38.4$

4. RESULTS AND DISCUSSION

As shown in Fig. 6, the three-dimensional near-field pattern of the proposed array with different distributions of excitations is tested. The default size of the observation surface is 120 mm × 120 mm, and the step size of the stepper is set to 2 mm. Fig. 7 gives the contour plots of the simulated and measured electric field intensities in different coordinate planes when the center of the sphere is located at P1, with the simulated results shown in Figs. 7(a), (b), and (c) and the measured results shown in Figs. 7(d), (e), and (f).

According to the simulation results, the synthesized 3 dB electric field in the center area of the transmitting array at the target height of 75 mm is a quasi-circular distribution, and the diameters are all about 60 mm in three observation planes. For the measured results in three planes, it can be seen that the actual distribution tends to be an ellipsoid one, whose major and minor axes are about 65 mm and 55 mm.

In order to better reveal the change of electric field, three straight lines passing the center of the sphere are drawn in the direction of the coordinate axis, and the changes in the electric field on the straight lines can be clearly observed. Fig. 8 shows the normalized electric field intensity on different lines. The 3 dB ranges of electric field distributed along the x-axis, y-axis, and z-axis are found to be 63 mm, 66 mm, and 62 mm according to the full-wave simulations. It can be seen from Fig. 8 that the normalized electric field intensity distributions along the three lines are nearly equal, which proves that the electric field is approximately sphere-shaped. The measured electric field distribution on the three

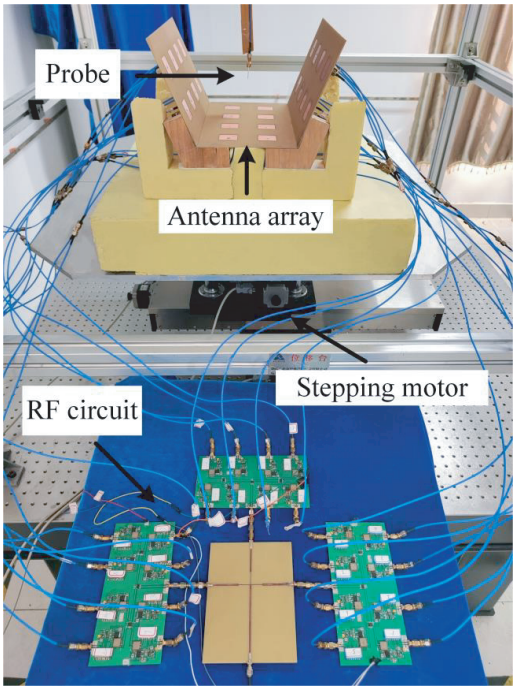

Figure 6. Photograph of the proposed 3D near-field shaping antenna array system.

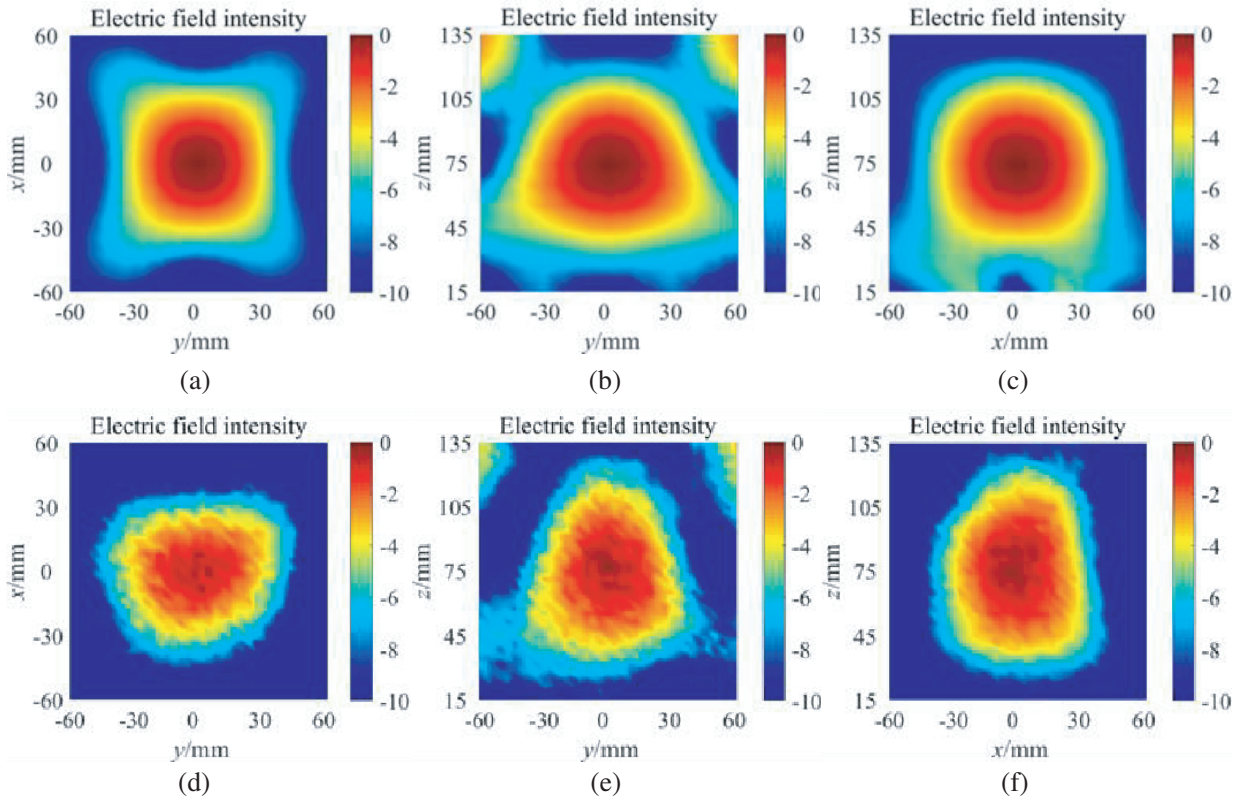

Figure 7. Contour plots of the normalized simulated and measured electric field intensities when the target spherical center is at P1. Simulated results in (a) xy-plane, (b) yz-plane, (c) xz-plane. Measured results in (d) xy-plane, (e) yz-plane, (f) xz-plane.

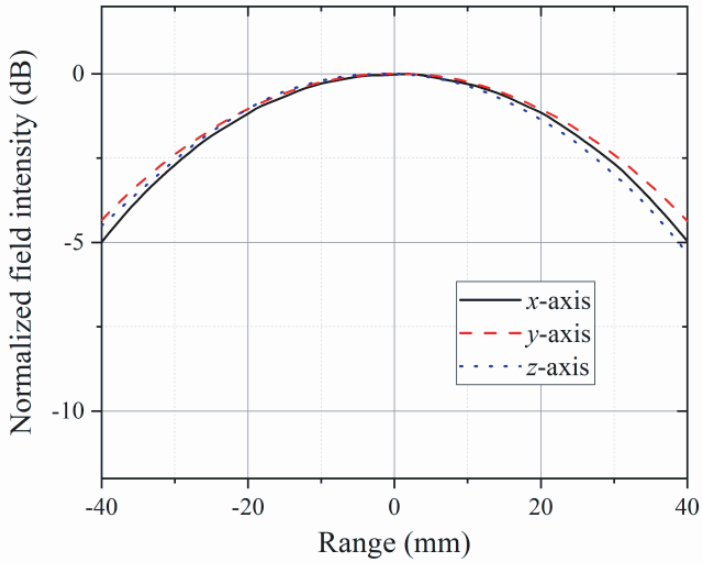

Figure 8. Normalized electric field intensity on three different lines.

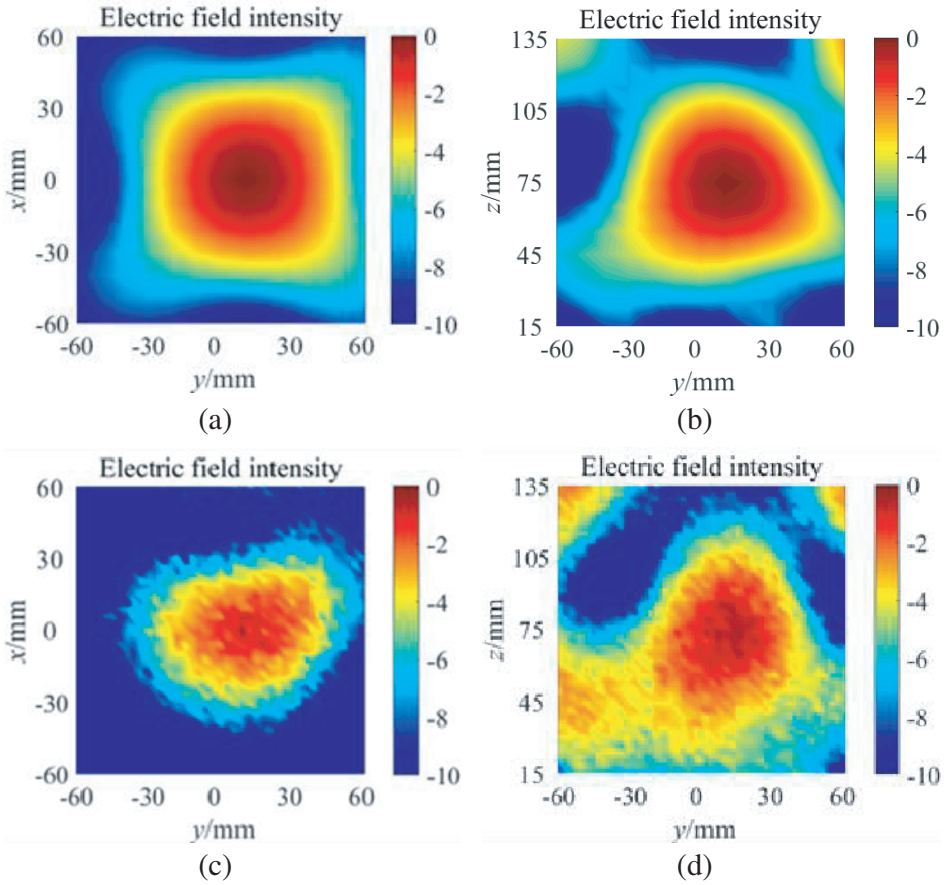

Figure 9. Contour plots of the normalized simulated and measured electric field intensities when the target spherical center is at P2. Simulated results in (a) xy-plane, (b) yz-plane. Measured results in (c) xy-plane, (d) yz-plane.

planes is ellipsoidal, with long and short axes of approximately 65 mm and 55 mm, respectively.

When the electric field positions generated by the transmitting array are expected at off-center positions of P2 and P3, the corresponding contour plots are shown in Fig. 9 and Fig. 10, respectively. The simulated results all show a spherical distribution, with a 10 mm offset in the desired direction achieved. The measured results show an ellipsoidal distribution, also achieving a 10 mm deviation in the desired direction. The actual measured electric field distribution agrees with the simulations, both achieving an offset of 10 mm in the desired direction. But the measured electric field distribution shape deviates from the preset sphere shape.

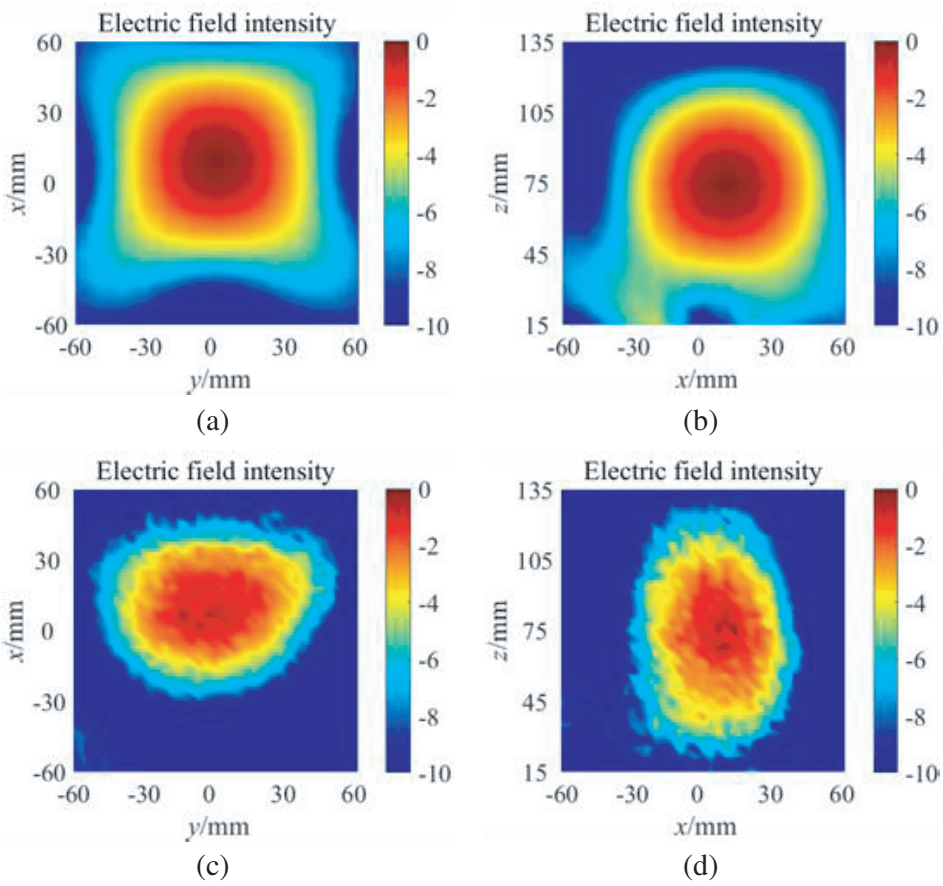

Figure 10. Contour plots of the normalized simulated and measured electric field intensities when the target spherical center is at P3. Simulated results in (a) xy-plane, (b) xz-plane. Measured results in (c) xy-plane, (d) xz-plane.

From the results presented above, it can be seen that the transmitting array antenna is able to achieve a preset 3D shape of the electric field distribution as well as a preset offset distance in the desired direction. Due to the measurement, the measured electric field distribution shape deviated from the preset sphere shape.

Two main reasons may account for the slight deviation between the measured and simulated results. First, when the electric field distribution in space is measured, the movement of test platform and the test probe may have a small shake during the process of acceleration and braking, leading to the deviation of the measured electric field distributions from the simulations. Second, the excitations generated by the RF feeding circuits cannot be exactly the same as the simulated excitations, which may also affect the test results.

5. CONCLUSION

In summary, a three-dimensional near-field pattern shaping antenna array based on WCMMPTE is proposed in this paper. By setting proper constraints for the electric field distribution of several selected points within the target area and calculating the array excitation by WCMMPTE, the electric field distribution of the preset 3D shape is achieved with the power maximally concentrated into this area at the same time. A 24-element array is designed and fabricated to validate the three-dimensional near-field shaping performance. Experiment results indicate that a spherical distribution of 3 dB electric field at center or off-center can be achieved at the target height of 75 mm. Furthermore, the measured 3 dB ranges along x-axis, y-axis, and z-axis for the spherical distribution at center and off-center are found to be (56 mm, 55 mm, 64 mm) and (52 mm, 60 mm, 65 mm), respectively, and the measured and simulated electric field distributions are in good agreement. By changing the selected points, precise control of the three-dimensional spatial electric field strength can by enabled by the proposed near-field shaping antenna array. The proposed concept can be applied in microwave hyperthermia, RFID system, and other near-field applications.

ACKNOWLEDGMENT

This work was supported by the National Natural Science Foundation of China under Grant 62101276; in part by the National Natural Science Foundation of China under Grant 61971231; and in part by the Natural Science Foundation of the Jiangsu Higher Education Institutions of China under Grant 21KJB510002.

REFERENCES

1. Yang, X., W. Geyi, and H. Sun, "Optimum design of wireless power transmission system using microstrip patch antenna arrays," *IEEE Antennas and Wireless Propagation Letters*, Vol. 16, 1824–1827, 2017.
2. Cai, X., X. Gu, and W. Geyi, "Optimal design of antenna arrays focused on multiple targets," *IEEE Transactions on Antennas and Propagation*, Vol. 68, No. 6, 4593–4603, Jun. 2020
3. Buffi, A., A. A. Serra, P. Nepa, H.-T. Chou, and G. Manara, "A focused planar microstrip array for 2.4 GHz RFID READERS," *IEEE Transactions on Antennas and Propagation*, Vol. 58, No. 5, 1536–1544, May 2010.
4. Tanter, M., J.-L. Thomas, and M. Fink, "Focusing through skull with time reversal mirrors. Application to hyperthermia," *IEEE Ultrasonics Symposium, Proceedings*, Vol. 2, 1289–1293, 1996.
5. Stang, J., M. Haynes, P. Carson, and M. Moghaddam, "A preclinical system prototype for focused microwave thermal therapy of the breast," *IEEE Transactions on Biomedical Engineering*, Vol. 59, No. 9, 2431–2438, Sep. 2012.
6. Tofigh, F., J. Nourinia, M. Azarmanesh, and K. M. Khazaei, "Near-field focused array microstrip planar antenna for medical applications," *IEEE Antennas and Wireless Propagation Letters*, Vol. 13, 951–954, 2014.
7. Nguyen, P. T., A. Abbosh, and S. Crozier, "Three-dimensional microwave hyperthermia for breast cancer treatment in a realistic environment using particle swarm optimization," *IEEE Transactions on Biomedical Engineering*, Vol. 64, No. 6, 1335–1344, Jun. 2017.
8. He, X., W. Geyi, and S. Wang, "Optimal design of focused arrays for microwave-induced hyperthermia," *IET Microwaves, Antennas & Propagation*, Vol. 9, No. 14, 1605–1611, Nov. 2015.
9. He, X., W. Geyi, and S. Wang, "A hexagonal focused array for microwave hyperthermia: Optimal design and experiment," *IEEE Antennas and Wireless Propagation Letters*, Vol. 15, 56-59, 2016.
10. Fink, M., "Time reversal of ultrasonic fields. I. Basic principles," *IEEE Transactions on Ultrasonics Ferroelectrics & Frequency Control*, Vol. 39, No. 5, 555–566, Sept. 1992.
11. Iero, D. A. M., L. Crocco, and T. Isernia, "Thermal and microwave constrained focusing for patient-specific breast cancer hyperthermia: A robustness assessment," *IEEE Transactions on Antennas and Propagation*, Vol. 62, No. 2, 814–821, Feb. 2014.

12. Nguyen, P. T., A. Abbosh, and S. Crozier, "Three-dimensional microwave hyperthermia for breast cancer treatment in a realistic environment using particle swarm optimization," *IEEE Transactions on Biomedical Engineering*, Vol. 64, No. 6, 1335–1344, Jun. 2017.
13. Buffi, A., P. Nepa, and G. Manara, "Design criteria for near-field-focused planar arrays," *IEEE Antennas and Propagation Magazine*, Vol. 54, No. 1, 40–50, Feb. 2012.
14. Blanco, D., J. L. Gómez-Tornero, E. Rajo-Iglesias, and N. Llombart, "Radially polarized annular-slot leaky-wave antenna for three-dimensional near-field microwave focusing," *IEEE Antennas and Wireless Propagation Letters*, Vol. 13, 583–586, 2014.
15. Chou, H.-T., M. R. Pino, P. Nepa, and C.-Y. Liu, "Near-field focused subarrays in a multi-panel configuration," *IEEE Access*, Vol. 7, 143097–143108, 2019.
16. Zhao, D. and M. Zhu, "Generating microwave spatial fields with arbitrary patterns," *IEEE Antennas and Wireless Propagation Letters*, Vol. 15, 1739–1742, 2016.
17. Bellizzi, G. G., D. A. M. Iero, L. Crocco, and T. Isernia, "Three-dimensional field intensity shaping: The scalar case," *IEEE Antennas and Wireless Propagation Letters*, Vol. 17, No. 3, 360–363, Mar. 2018.
18. Geyi, W., "The method of maximum power transmission efficiency for the design of antenna arrays," *IEEE Open Journal of Antennas and Propagation*, Vol. 2, 412–430, 2021.
19. Cai, X. and W. Geyi, "An optimization method for the synthesis of flat-top radiation patterns in the near- and far-field regions," *IEEE Transactions on Antennas and Propagation*, Vol. 67, No. 2, 980–987, Feb. 2019.